J Membrane Biol (2009) 227:25–37
DOI 10.1007/s00232-008-9141-5

The Effects of GPX-1 Knockout on Membrane Transport and Intracellular Homeostasis in the Lens

Huan Wang · Junyuan Gao · Xiurong Sun · Francisco J. Martinez-Wittinghan · Leping Li · Kulandaiappan Varadaraj · Melissa Farrell · Venkat N. Reddy · Thomas W. White · Richard T. Mathias

Received: 14 August 2008 / Accepted: 5 November 2008 / Published online: 9 December 2008
© Springer Science+Business Media, LLC 2008

Abstract Glutathione peroxidase-1 (GPX-1) is an enzyme that protects the lens against H_2O_2-mediated oxidative damage. The purpose of the present study was to determine the effects of GPX-1 knockout (KO) on lens transport and intracellular homeostasis. To investigate these lenses we used (1) whole lens impedance studies to measure membrane conductance, resting voltage and fiber cell gap junction coupling conductance; (2) osmotic swelling of fiber cell membrane vesicles to determine water permeability; and (3) injection of Fura2 and Na^+-binding benzofuran isophthalate (SBFI) into fiber cells to measure $[Ca^{2+}]_i$ and $[Na^+]_i$, respectively, in intact lenses. These approaches were used to compare wild-type (WT) and GPX-1 KO lenses from mice around 2 months of age. There were no significant differences in clarity, size, resting voltage, membrane conductance or fiber cell membrane water permeability between WT and GPX-1 KO lenses. However, in GPX-1 KO lenses, coupling conductance was 72% of normal in the outer shell of differentiating fibers and 45% of normal in the inner core of mature fibers. Quantitative Western blots showed that GPX-1 KO lenses had about 50% as much labeled Cx46 and Cx50 protein as WT, whereas they had equivalent labeled AQP0 protein as WT. Both Ca^{2+} and Na^+ accumulated significantly in the core of GPX-1 KO lenses. In summary, the major effect on lens transport of GPX-1 KO was a reduction in gap junction coupling conductance. This reduction affected the lens normal circulation by causing $[Na^+]_i$ and $[Ca^{2+}]_i$ to increase, which could increase cataract susceptibility in GPX-1 KO lenses.

Keywords Glutathione peroxidase-1 · Connexin 46 · Connexin 50 · Aquaporin 0 · Intracellular calcium · Intracellular sodium

H. Wang · J. Gao · X. Sun · F. J. Martinez-Wittinghan · L. Li · K. Varadaraj · M. Farrell · T. W. White · R. T. Mathias (✉)
Department of Physiology and Biophysics, SUNY at Stony Brook, Stony Brook, NY 11794-8661, USA
e-mail: richard.mathias@sunysb.edu

V. N. Reddy
Biomedical Sciences, Eye Research Institute, Oakland University, Rochester, MI 48309-4480, USA

Introduction

The fully developed lens can be divided into three domains (see Fig. 1): an anterior layer of epithelial cells (E), peripheral differentiating fibers (DF) and central mature fibers (MF). The epithelial cells elongate at the equator and at the E-to-DF transition form new fiber cells, which have a different complement of cytoplasmic and membrane proteins from epithelial cells. The DF-to-MF transition occurs at about 15% of the distance into a lens, where there is a zone of extensive membrane protein cleavage and loss of organelles. Thus, MF cells lack organelles and do not have the ability to synthesize new proteins, so if MF proteins are damaged, they cannot be replaced (Kuszak and Rae 1982; Bassnett and Beebe 1992; Mathias et al. 1997).

Gap junction channels are formed by the docking of two integral membrane hemichannels in adjacent cells. Each hemichannel is composed of six connexin (Cx) monomers. In the lens, epithelial cells express Cx43 and Cx50; but at the E-to-DF transition, expression of Cx43 is lost and expression of Cx46 begins (see Fig. 1). Both DF and MF contain Cx46 and Cx50 but with different structural and functional properties (Goodenough et al. 1996; Kumar and Gilula 1996). In DF both connexins appear to form functional channels, which contribute about equally to the total

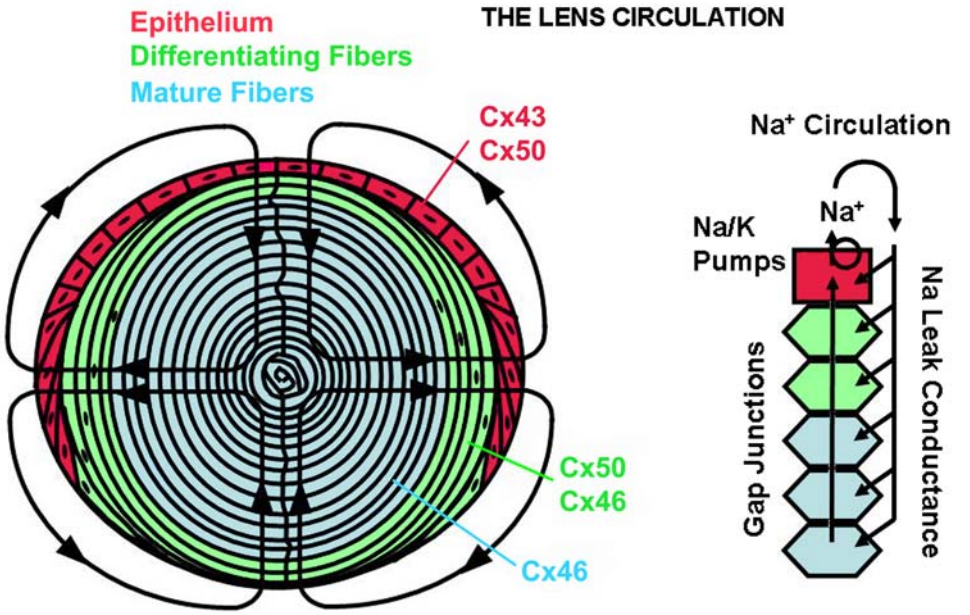

Fig. 1 The structure of the lens, its internal circulatory system and the distribution of functional gap junction connexins

coupling conductance, whereas in MF functional Cx50 channels appear to be lost (Gong et al. 1998; Baldo et al. 2001; Martinez-Wittinghan et al. 2004), possibly due to cleavage at the DF-to-MF transition (DeRosa et al. 2006). Thus, Cx46 channels provide communication between the central MF and the surface of the lens (see Fig. 1) and appear to be a critical component of the lens circulation (Gao et al. 2004; Mathias et al. 2007).

Robinson and Patterson (1982–1983) first found there is a circulating current in rat lenses. Other investigators measured similar currents in lenses from frogs and rabbits (Robinson and Patterson 1982–1983; Parmelee 1986; Candia and Zamudio 2002). Hence, the circulating current appears to be ubiquitous. The lines of current flow are superimposed on the schematic of a lens shown in Fig. 1. There is a net inward current at both poles and a net outward current at the equator. Mathias and Rae (1985) suggested the current was carried by Na^+, the principal extracellular cation. Their model for the circulating currents is shown in the right-hand side of Fig. 1: Na^+ enters the lens through the extracellular spaces, where it flows toward central fiber cells. As it moves into the lens, it flows down its transmembrane electrochemical gradient into fiber cells. Once in the intracellular compartment, the flow reverses direction and Na^+ moves toward the lens surface from cell to cell through gap junctions. The interesting pole-to-equator circulation occurs because DF gap junction coupling conductance is concentrated in the equatorial region (Baldo and Mathias 1992). Thus, the outward intracellular current is directed to the equator by the pattern of gap junction coupling. Moreover, Na/K pumps are concentrated in equatorial epithelial cells (Candia and Zamudio 2002; Gao et al. 2000; Delamere and Tamiya 2004), where they transport Na^+ out of the lens.

The Na^+ flux represents a net flux of solute (Mathias 1985), which is thought to generate water flow that follows the same pattern (Mathias et al. 1997; Candia and Alverez 2006; Mathias et al. 2007). The water movement creates an internal microcirculatory system for the avascular lens. The inwardly directed flow of extracellular fluid carries essential molecules, including metabolites and antioxidants, to the centrally located MF. The MF have membrane transporters to take up these molecules, and those that have been identified are generally Na^+-dependent cotransporters, which rely on the transmembrane electrochemical gradient for Na^+ to drive uptake of the nutrient or antioxidant (reviewed in Mathias et al. 2007).

A cation such as Ca^{2+} is expected to circulate in a manner similar to Na^+, so Ca^{2+} homeostasis in the lens should depend on gap junction coupling. Gao et al. (2004) showed that in Cx46 knockout (KO) mice MF gap junction coupling is lost, the Ca^{2+} efflux pathway is therefore lost and Ca^{2+} accumulates in the MF. They also showed that in lenses in which Cx46 is knocked into the Cx50 gene locus, MF gap junction coupling doubles and the center-to-surface diffusion gradient for Ca^{2+} is halved. These data are consistent with the above-described model for the circulation of ions through the lens, though this particular study did not measure the effect of changes in gap junction coupling on center-to-surface Na^+ gradients.

Central cataracts have been reported in mice lacking the enzyme glutathione peroxidase-1 (GPX-1), which protects the lens against H_2O_2-mediated oxidative damage (Reddy 1990; Reddy et al. 2001). Although H_2O_2 is not a radical

and is less reactive than reactive oxygen species (ROS), it is relatively stable, which allows it to move and pass rapidly through cell membranes (Spector 1995). H_2O_2-induced damage is prevented by a powerful system in which catalase, glutathione reductase and GPX are the key enzymes. There are four known forms of GPX (GPX1-4), but GPX-1 is the only cytoplasmic form. KO of GPX-1 provides a useful model to study the direct role of oxidative damage in generating age-dependent cataract formation. In KO animals younger than 5 months, no lenses develop cataracts. However, the fraction increases with age and is essentially 100% in lenses from mice older than 15 months. No control lenses have opacities when mice are younger than 15 months (Reddy et al. 2001).

The purpose of the current study was to see if we could detect changes in lens membrane transport that are induced by KO of GPX-1 yet precede the formation of a cataract. The only significant change we observed was a reduction in gap junction coupling conductance that appears to be due to a reduction in the amount of functional Cx46 and Cx50 protein. The work of Gao et al. (2004) and the above-described model of the lens circulation suggest the reduction in gap junction coupling should cause accumulation of Ca^{2+} and Na^{+} in central fiber cells. We therefore examined intracellular homeostasis in lenses from GPX-1 KO to see if reductions in gap junction coupling indeed caused accumulation of circulating ions in the central fiber cells.

Materials and Methods

Unless otherwise noted, chemicals and supplies were acquired from Sigma (St. Louis, MO).

Solutions

Tyrode solution contained (in mM) 137.7 NaCl, 5.4 KCl, 2.3 NaOH, 2 $CaCl_2$, 1 $MgCl_2$, 10 glucose and 5 HEPES (pH 7.4 with NaOH).

Pipette solution for Na^{+} measurement contained (in mM) 83 K-aspartic acid, 17 KCl, 5 HEPES and 10 choline-Cl (pH 6.9 with KOH).

Pipette solution for Ca^{2+} measurement contained (in mM) 83 K-aspartic acid, 17 KCl, 5 HEPES and 10 $NaCH_3OSO_3$ (pH 6.9 with KOH).

Ca^{2+} buffer solution contained (in mM) 100 KCl, 30 MOPS, 10 K_2EGTA and 1–10 CaEGTA (pH 7.2) (Molecular Probes, Eugene, OR).

Vesicle solution contained (in mM) 150 NaCl, 7 KCl, 1 $MgCl_2$, 5 glucose and 5 HEPES (pH 7.2). Calculated osmolarity was 324 mM.

Hypertonic vesicle solution contained (in mM) 225 NaCl, 7 KCl, 1.5 $MgCl_2$, 7.5 glucose and 7.5 HEPES (pH 7.2). Calculated osmolarity was 487 mM.

Impedance Studies

These studies were performed as previously described (Gong et al. 1998; Baldo et al. 2001; Mathias et al. 1991). Briefly, WT and GPX-1 KO mice of mixed genetic background (C57/J129) were killed by intraperitoneal injection of sodium pentobarbital solution (100 mg/kg of weight). The eyes were removed and the lenses dissected in a Sylgard (Dow Corning, Midland, MI)–lined dish in normal Tyrode solution initially warmed to 37°C. First, the cornea and iris were removed and the optic nerve was cut off; then, the sclera was cut into four flaps from the lens posterior surface in order to mount the lens on the Sylgard base.

Microelectrodes were shielded with silver paint (SPI Supplies, West Chester, PA) to within a few hundred micrometers of the tip and coated with silicone. The function of the silicone (Dow Corning, Midland, MI) was to insulate the silver paint from the bath. One microelectrode (current electrode) was used to inject a random current of selected bandwidth into a central fiber cell. The second microelectrode (voltage electrode) was used to record the induced voltage. The lens was mounted in a perfusion chamber in which the external solutions were prewarmed to 37°C. The voltage electrode was placed into the lens at different depths. Impedance was analyzed and calculated by a fast Fourier analyzer (model 5420A; Hewlett-Packard, Palo Alto, CA). Series resistance (R_s), defined in Eqs. 1–3, was used to evaluate gap junction coupling. To test pH gating properties, the lens was superfused with Tyrode solution that had been bubbled with 100% CO_2 for about 10 min (Martinez-Wittinghan et al. 2004).

Model of Gap Junctional Coupling

In spherically symmetric syncytial tissue, equations for radial current flow were derived by Eisenberg et al. (1979) and modified by Mathias et al. (1991). At sinusoidal frequencies approaching 1 kHz, the induced intracellular and extracellular voltages become nearly identical and are given by IR_s, where I is the injected current and R_s (Ω) is the cumulative series resistance between the point of voltage recording (r cm from the center) and the lens surface (a cm from the center). R_s is directly proportional to R_P, where R_P (Ωcm) is the parallel resistivity of the intracellular and extracellular compartments (Gong et al. 1998; Baldo et al. 2001; Mathias et al. 1991).

$$R_s = \frac{1}{4\pi}\int_r^a \frac{R_p}{\rho^2}d\rho \qquad R_p = \frac{R_i R_e}{R_i + R_e} \tag{1}$$

The effective intracellular resistivity, R_i, is due mainly to the gap junctional coupling resistance, whereas the effective extracellular resistivity, R_e, depends on the tortuosity and volume fraction of small extracellular clefts. In normal physiological conditions, R_e is much higher than R_i; therefore, $R_P \approx R_i$. For simplicity and lack of contrary data, we assume that R_e is uniform, whereas we have measured that R_i changes at the DF-to-MF transition (defined as $r = b$). Integrating Eq. 1 gives the following:

$$R_s = \frac{R_{DF}}{4\pi}\left(\frac{1}{r} - \frac{1}{a}\right) \quad b \le r \le a \tag{2}$$

$$R_s = \frac{R_{DF}}{4\pi}\left(\frac{1}{b} - \frac{1}{a}\right) + \frac{R_{MF}}{4\pi}\left(\frac{1}{r} - \frac{1}{b}\right) \quad r \le b \tag{3}$$

where R_{DF} is R_i in DF and R_{MF} is R_i in MF.

Fiber Cell Membrane Water Permeability

Fiber cell membrane vesicles from DF were prepared as described in Varadaraj et al. (1999). Vesicles did not form from MF, so the studies here report p_m for DF only. Vesicles were placed in a perfusable bath where the solution osmolarity was switched between 324 and 487 mM. Images of cross-sectional area were recorded using an Olympus (Tokyo, Japan) CKX41 inverted microscope equipped with a video camera. Images were digitized on the computer using a video frame-grabber and Inspector 6 software (Matrox, Dorval, Quebec, Canada). Volume of the vesicles was estimated based on spherical geometry. Vesicle p_m values were calculated from the initial rate of volume change (Varadaraj et al. 1999).

Western Blotting

Lenses from 4-month-old mice were dissected, and equal wet weights were homogenized in 7 M urea, 50 mM Tris-HCl (pH 7.4). After a 1:1 dilution with distilled H_2O and centrifugation at 14,000*g* for 20 min at room temperature, the insoluble fraction was resuspended in 50 mM Tris-HCl (pH 7.4) and centrifuged at 100,000*g* for 30 min at 4°C. Pellets were resuspended in sample buffer and stored at −80°C. Equal aliquots of samples from each genotype were electrophoresed on 10% SDS-polyacrylamide gels and transferred to nitrocellulose membranes (Schleicher and Schuell BioScience, Keene, NH). Equal protein loading and efficiency of protein transfer for the three genotypes was verified by staining filters with Ponceau S (Sigma). Blots were then immunostained with antibodies specific for the carboxy tail of Cx46 (Paul et al. 1991), the cytoplasmic loop of Cx46 (Gong et al. 1997), the carboxy tail of Cx50 (Santa Cruz Biotechnology, Santa Cruz, CA) or the fiber cell membrane water channel aquaporin 0 (AQP0; generously provided by Dr. J Horwitz, Jules Stein Eye Institute, UCLA, Los Angeles, CA), followed by horseradish peroxidase-conjugated secondary antibodies using Western Blotting Luminol Reagent as a chemiluminescent substrate (Santa Cruz Biotechnology, Santa Cruz, CA). MagicMark (Invitrogen, Carlsbad, CA) protein standards were used as molecular weight markers. Blots were digitized and band intensities were quantified using Kodak 1D Image Analysis software (Eastman Kodak, Rochester, NY). Values were normalized to the mean value of band intensity in the wild-type (WT) sample.

Measurement of $[Ca^{2+}]_i$ within the Lens

Intracellular Ca^{2+} was measured using a dual wavelength spectrometer system as described by Gao et al. (2004). Fura2 (0.2 mM) was dissolved in the pipette solution, which was injected into lens fiber cells at different depths. After a few minutes, diffusion slowed to an undetectable rate; then, the images were digitally captured and the ratios of emission at 360/380 excitation calculated. By using Ca^{2+}-dependent calibration curves from seven depths into the lens, as described by Gao et al. (2004), the ratios were converted into Ca^{2+} concentrations.

Measurement of $[Na^+]_i$ within the Lens

Na^+ measurements were basically the same as Ca^{2+} measurements, except that Na^+-binding benzofuran isophthalate (SBFI) was the Na^+ probe. SBFI was dissolved in the pipette solution. This solution was injected into fiber cells at different depths in the lens. The ratios of emission at 360/380 nm excitation were compared to Na-calibration curves that were determined at seven depths into the lens, as was done for Ca^{2+}.

Data Analysis

Data were analyzed with Sigma Plot 2000 (SPSS Science, Chicago, IL), Sigmastat 3.0 (SPSS Science) and Microsoft (Redmond, WA) Excel (2003). All values are given as means ± standard deviations. Two group comparisons were made using Student's *t*-test; $P < 0.05$ was considered statistically significant.

Theory

The purpose of the modeling presented here was to examine the relationship between gap junction coupling

conductance, transmembrane ionic current and the intracellular electrodiffusion gradient driving ionic current from the center to the surface of the lens. Intracellular fluid flow was neglected as its effect is expected to be small (Mathias et al. 2007) and is not well characterized. Moreover, in this model, transmembrane ionic current is assumed to be uniform throughout the lens. The model is not arbitrary, however, as it is based on the physical structure of the lens and the thermodynamics of ion fluxes.

Previous models (Mathias 1985; Mathias et al. 1997) have focused on net intracellular radial current flow (i_r A/cm^2), given by the sum of $i_{Na} + i_K + i_{Cl}$, rather than individual ionic currents. These models invoked macroscopic electroneutrality and approximate osmotic equilibrium to simplify the equations. They showed that i_r is determined by Ohm's law in a continuum. Conservation of charge requires the divergence in radial current equal the net transmembrane current (i_m A/cm^2, current leaving a cell is defined as positive) scaled by the surface area of membrane per unit volume of tissue (S_m/V_T cm^{-1}):

$$\frac{S_m}{V_T} i_m = \frac{1}{R_{MF}} \frac{1}{r^2} \frac{d}{dr} \left(r^2 \frac{d\psi_i}{dr} \right) \tag{4}$$

The intracellular voltage is ψ_i (volts) and the effective intracellular resistivity in MF is R_{MF} (Ω cm). Since the majority of the lens is MF, we neglect the change in resistivity at the MF-to-DF transition, which has a very small effect on the predicted voltage. We therefore integrate Eq. 4 to obtain a relationship between the voltage at the lens surface—$\psi_i(a)$ volts—and the voltage gradient between the lens surface and center—$\Delta\psi_i$ volts:

$$\psi_i(r) = \psi_i(a) + \Delta\psi_i(1 - r^2/a^2) \tag{5}$$

where

$$\Delta\psi_i = -\frac{S_m}{V_T} \frac{a^2 R_{MF} i_m}{6} \tag{6}$$

As can be seen in Eq. 6, $\Delta\psi_i$ is directly proportional to R_{MF}, which is inversely proportional to gap junction coupling conductance. Thus, if i_m is constant but the coupling conductance is halved, the voltage gradient should double. In MF, i_m is inward or negative, so $\Delta\psi_i \approx 10$ mV is positive and in small WT mouse lenses the voltage varies from $\psi_i(a) \approx -70$ mV at the surface to -60 mV at the center (Baldo et al. 2001).

Standing intracellular voltage gradients depend on the net current flow of all ions, but they also affect the flow of each individual ion. The intracellular concentration of ion X will be denoted $[X]_i$ (moles/cm^3), where in this analysis X is either Na^+ or Ca^{2+}. The effective intracellular diffusion coefficient for ion X, D_X (cm^2/s), is directly proportional to the intracellular coupling conductance. Define the normalized intracellular voltage as follows:

$$\varphi_X = \frac{FZ_X}{RT} \psi_i \tag{7}$$

The intracellular radial current for each ion is determined by the Nernst–Planck equation $i_{rX} = -FZ_X D_X \left(\frac{d[X]_i}{dr} + [X]_i \frac{d\phi_X}{dr} \right)$, where i_{rX} is the radial current and the divergence in radial current equals the transmembrane current:

$$\frac{S_m}{V_T} i_X = FZ_X D_X \frac{1}{r^2} \frac{d}{dr} r^2 \left(\frac{d[X]_i}{dr} + [X]_i \frac{d\varphi_X}{dr} \right) \tag{8}$$

Inserting Eq. 5 into Eq. 8 yields a linear differential equation that can be solved analytically:

$$[X]_i(r) = [X]_i(a) \exp\{-\Delta\varphi_X(1 - r^2/a^2)\} + \frac{\delta[X]_i}{\Delta\varphi_X} \left(1 - \exp\{-\Delta\varphi_X(1 - r^2/a^2)\}\right) \tag{9}$$

where

$$\delta[X]_i = -\frac{S_m}{V_T} \frac{a^2 i_X}{6FZ_X D_X} \tag{10}$$

The relationship between coupling conductance and diffusion gradients is not transparent from the solution given by Eq. 9. The argument of the exponential in Eq. 9 is always less than 1; thus, a power series expansion should be reasonably accurate. Such an expansion yields

$$[X]_i(r) = [X]_i(a) + \Delta[X]_i \left(1 - r^2/a^2\right) \tag{11}$$

where

$$\Delta[X]_i = \delta[X]_i - [X]_i(a)\Delta\varphi_X \tag{12}$$

In the absence of a voltage gradient ($\Delta\Phi_X$), the concentration gradient would equal $\delta[X]_i$; but because of the voltage gradient, part of the flux is carried by conduction and the concentration gradient is reduced. However, both $\delta[X]_i$ and $\Delta\Phi_X$ are inversely proportional to coupling conductance; thus, $\Delta[X]_i$ is also inversely proportional to coupling conductance. If the coupling conductance is reduced by half and if the transmembrane current i_X does not change, the concentration gradient should double.

As can be seen in Eq. 10, $\delta[X]_i$ is directly proportional to i_X; however, it is not clear how the term $[X]_i(a)$ relates to i_X. To determine the relationship, consider the total flux leaving cells at the lens surface, I_X (A).

$$I_X = \frac{4}{3} \pi a^3 \frac{S_m}{V_T} i_X \tag{14}$$

This flux is carried by active transporters, such as the Na/K-ATPase, whose rate of transport is approximately proportional to the concentration of substrate, in this example $[Na^+]_i$. Thus if $I_X = k_X[X]_i(a)$, then $[X]_i(a)$ is approximately determined by

$$[X]_i(a) = \frac{4}{3}\pi a^3 \frac{S_m}{V_T}\frac{i_X}{k_X} \quad (15)$$

Insofar as k_X does not change, $[X]_i(a)$ will be approximately proportional to i_X.

Summary

Equation 11 shows that the concentration of ion X at any radial location r depends on two parameters: (1) the concentration of ion X at the surface, $[X]_i(a)$, which is directly proportional to fiber cell membrane current, inversely proportional to the rate of active transport by surface cells but independent of coupling conductance, and (2) the difference between the concentration at the lens surface and center, $\Delta[X]_i$, which is directly proportional to membrane current, inversely proportional to coupling conductance and weakly dependent on active transport by cells at the lens surface. Equation 11 was used to fit the $[Ca^{2+}]_i$ and $[Na^+]_i$ data reported in "Results."

Results

Lenses from 2-month-old GPX-1 KO mice were not significantly different in size from WT: GPX-1 KO radius $a = 0.105 \pm 0.003$ cm, $n = 25$; WT $a = 0.104 \pm 0.001$ cm, $n = 15$. In addition, insofar as could be determined through light microscopy, GPX-1 KO lenses maintained clarity comparable to that of WT. The intracellular voltage measured near the lens surface was not significantly different in WT (69 ± 2 mV, $n = 15$) vs. GPX-1 KO (68 ± 3 mV, $n = 8$). The average input resistance (R_{IN}) measured near the lens surface was also not significantly different, with $R_{IN} = 3.5 \pm 0.4$ KΩ in KO lenses vs. 3.7 ± 0.5 KΩ in WT. These data suggest KO of GPX-1 has no significant effect on membrane conductance at this early age.

Gap Junction Coupling

In DF, the coupling conductance varies from equator to poles, with the lowest values at the poles, whereas in MF, cell-to-cell coupling is relatively uniform (Baldo and Mathias 1992). All of our data were recorded at 45° from the posterior pole, where the current density and coupling conductance will be close to their angular averages. This section compares the average gap junction coupling conductance in GPX-1 KO lenses with that in WT lenses of mice at the same age.

Figure 2 shows R_S data from GPX-1 KO and WT lenses and the curve fit of Eqs. 2 and 3 to these data. R_s (Ω) represents the cumulative series resistance due to gap junctions between the surface of the lens and the point of recording. Given the larger R_S at all radial locations in the GPX-1 KO relative to WT lenses, it is qualitatively clear that there is less coupling in the KO lenses. At the DF-to-MF transition, the effective intracellular resistivity in either type of lens increases. This can be seen as a change in the slope of the smooth curves. Without this increase in resistivity at the DF-to-MF transition, the data in MF would fall above the model curve, with the fit becoming increasingly poor with depth. The graph is scaled to the relatively large resistance in MF, so the fit to the DF data look trivial. This is not the case however. The DF data are more accurate and therefore have a lower standard deviation than the MF data since errors in locating the voltage recording microelectrode increase with depth into the lens (as r gets smaller in Eq. 3). The value of R_{DF} is not affected by these uncertainties as it is determined before the value of R_{MF} can be estimated and, therefore, very well determined.

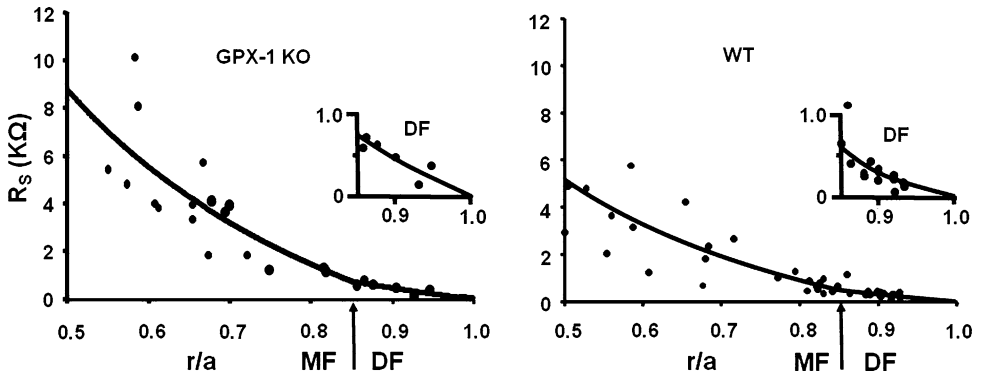

Fig. 2 The series resistance (R_S, KΩ) due to gap junction coupling between the point of recording r cm from the lens center and the surface of the lens at $r = a$ cm. The data are graphed as a function of the fractional distance from the lens center, r/a. *Insets* show expanded views of R_S in the DF. The resistance is clearly lower in WT than GPX-1 KO lenses, indicating less gap junction coupling conductance in the KO lenses. The best fit values of coupling conductance (S/cm^2 of cell-to-cell contact) used to generate the smooth curves were WT $G_{DF} = 0.96$ and $G_{MF} = 0.44$; GPX-1 KO $G_{DF} = 0.60$ and $G_{MF} = 0.26$

Table 1 Coupling conductance in lenses from 2-month-old GPX–1 KO and WT lenses

Coupling conductance (S/cm^2) of cell-to-cell contact	WT	GPX-1 KO	KO/WT
DF	0.83 ± 0.07	0.60 ± 0.09	0.72
MF	0.42 ± 0.08	0.19 ± 0.03	0.45

The coupling conductance per unit area of cell-to-cell contact was calculated for DF (G_{DF}) and MF (G_{MF}) from the R_{DF} and R_{MF} values. There were statistically significant differences in both G_{DF} and G_{MF} between 2-month-old WT and 2-month old GPX-1 KO lenses ($n = 10$ for G_{DF} and $n = 10$ for G_{MF})

The coupling conductance per unit area of cell-to-cell contact was calculated for DF ($G_{DF} = 1/wR_{DF}$) and MF ($G_{MF} = 1/wR_{MF}$), where R_{DF} and R_{MF} are defined in Eqs. 2 and 3 of "Materials and Methods," and $w \approx 3 \times 10^{-4}$ (cm) is the width of a fiber cell. At 2 months of age, in the absence of any cataract formation, statistically significant decreases in G_{DF} and G_{MF} were found when the GPX-1 gene was knocked out. Table 1 summarizes gap junction coupling in these lenses. The conductances in Table 1 were determined by curve fitting data from each lens studied, then averaging the values so that we could get standard deviations. These values are slightly different from those obtained by curve fitting Eqs. 2 and 3 to the raw data shown in Fig. 2 (see legend); however, the differences are small and the conclusions are exactly the same.

The data in Table 1 show that on average about 55% of MF channels have ceased to be functional in GPX-1 KO lenses, whereas only 28% of DF channels were lost. Presuming the loss of coupling conductance is due to oxidative damage, which should accumulate with time, one expects the older MF to suffer more damage than the newly formed DF. Indeed, there may be a continuous loss of coupling with depth/time, but our data are not sensitive enough to detect it.

Gap Junction Channel Gating

Gap junction channels made from most connexins show a decrease in conductance with a reduction in intracellular pH (Spray et al. 1981). However in the lens, MF coupling conductance, which depends on Cx46 channels, is pH-insensitive whereas DF coupling conductance, which depends on both Cx46 and Cx50 channels, is pH-sensitive (Mathias et al. 2007). Moreover, when Cx50 channels are knocked out (Baldo et al. 2001), pH gating is lost, or when they are blocked (Martinez-Wittinghan et al. 2006), pH sensitivity of DF channels is decreased in proportion to the degree of blockade. The stoichiometry of Cx46/Cx50 channels appears to be important for pH gating in the lens, such that selective damage to Cx50, but not Cx46, would alter pH-mediated gating.

To test pH gating properties, the lens was superfused with normal Tyrode solution that had been bubbled with 100% CO_2 (see "Materials and Methods"). When the voltage electrode was placed in the DF of GPX-1 KO lenses, there was a large increase in R_s (series resistance) when pH dropped (Fig. 3). This implies that DF gap junction channels are pH-sensitive. Since the DF channels retain normal pH sensitivity, these data suggest there are sufficient functional Cx50 channels to maintain normal gating.

When the point of voltage recording was in the MF, the percent increase in R_s was relatively small. As shown in Eq. 3, R_S depends on the cumulative resistance of DF in series with MF; and since coupling of MF is not pH-sensitive, the fractional increase in R_s measured in the MF will be small and dependent on uncoupling of DF (Mathias et al. 1991). Thus, pH gating properties of GPX-1 KO lenses were the same as those of control lenses, in which the DF gap junction channels are pH-sensitive and the MF gap junction channels are pH-insensitive.

Fiber Cell Membrane Water Permeability

Lens fiber cell membrane water permeability is mainly (~80%) due to AQP0 (Varadaraj et al. 1999; Shiels et al. 2001). Like the lens fiber cell connexins, AQP0 is subjected to cleavage in the older central fiber cells, and loss of its C terminus may cause loss of water permeability (Gonen et al. 2004). Thus, if GPX-1 KO had caused nonspecific oxidation of cytoplasmic domains of membrane proteins, the fiber cell membrane water permeability should be reduced in the GPX-1 KO relative to WT lenses.

Figure 4a shows a typical swelling assay of a fiber cell membrane vesicle when the bathing solution was switched from 487 to 324 mM. Based on the initial rate of swelling, the membrane water permeability (p_m cm/s) was calculated. These right side-out vesicles can be seen to form from membranes of isolated clumps of fiber cells peeled from the outer cortex of the lenses (Varadaraj et al. 1999). Fiber cells peeled from the nuclear region of these lenses do not produce vesicles; hence, we are reporting the water permeability of primarily DF. Figure 4b shows the average values of p_m as follows: WT $p_m = 28 \pm 3$ μm/s, GPX-1 KO $p_m = 24 \pm 5$ μm/s. These values are not statistically different; thus, AQP0 does not appear to have suffered significant oxidative damage in these young lenses.

Fiber Cell Membrane Protein Levels

The reductions in coupling conductance shown in Table 1 indicate there are fewer functional Cx46 and/or Cx50

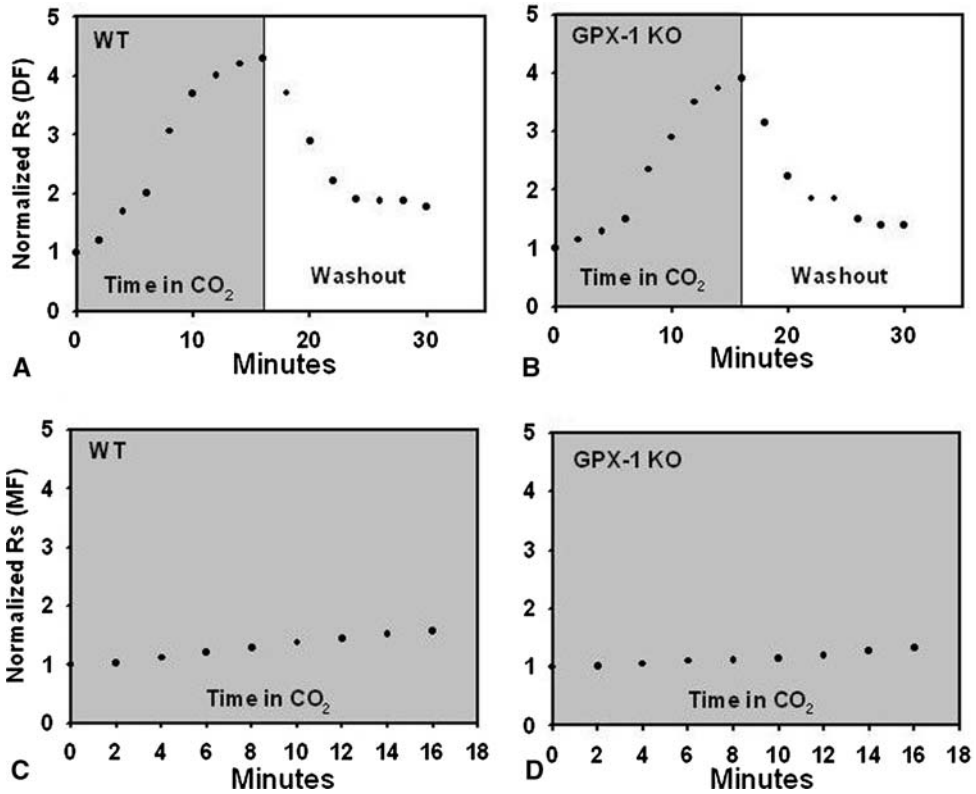

Fig. 3 Gating properties of gap junction channels in 2-month-old lenses. To test pH gating properties, the lens was superfused with Tyrode solution that had been bubbled with 100% CO_2 for about 10 min. **a** Gating of gap junction channels in DF of WT lenses. There was a large increase in R_S when pH dropped, indicating R_{DF} had increased significantly. **b** Gating properties of gap junction channels in DF of GPX-1 KO lenses. The data show a similar pattern of change in R_S as seen in WT lenses, suggesting no differences in DF gating. **c** Gating properties of gap junction channels in MF of 2-month-old WT lenses. When the point of voltage recording is in the MF, the increase in R_S depends on the series connection of R_{DF} and R_{MF}. The increase is relatively small, consistent with the increase of R_{DF} and not R_{MF}. These data imply that MF gap junction channels are not pH-sensitive. **d** Gating properties of gap junction channels in MF of 2-month-old GPX-1 KO lenses. The data show a similar pattern of change in R_S as seen in WT lenses, suggesting no differences in MF gating

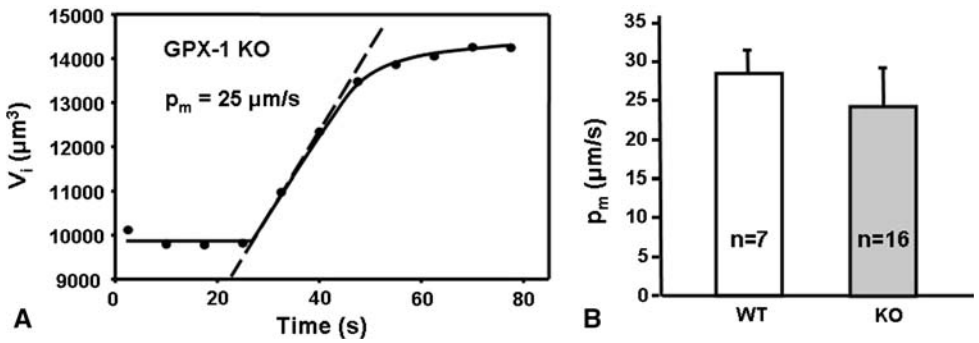

Fig. 4 Fiber cell membrane water permeability. **a** Typical swelling assay of a fiber cell membrane vesicle formed from isolated DF. This example was from a GPX-1 KO lens. *Dashed line* shows our estimate of the initial rate of volume change, which was used to calculate the water permeability, p_m. Both swelling and shrinking assays were used as the bath osmolarity was switched between 324 and 487 mM. **b** Average results showing the p_m of DF from GPX-1 KO and WT lenses. There is no statistically significant difference

channels in the KO lenses. This could be due to either closure of existing channels or degradation of Cx46 and/or Cx50 protein. We therefore performed quantitative Western blotting of Cx46 and Cx50 in lenses from WT and GPX-1 KO mice.

Figure 5 illustrates Western blots of the three major lens fiber membrane proteins, Cx46, Cx50 and AQP0. For Cx46, antibodies recognizing two different epitopes, the C terminus (Cx46 tail, Fig. 5a) and the inner cytoplasmic loop (Cx46 loop, Fig. 5b), were used. Since the C terminus

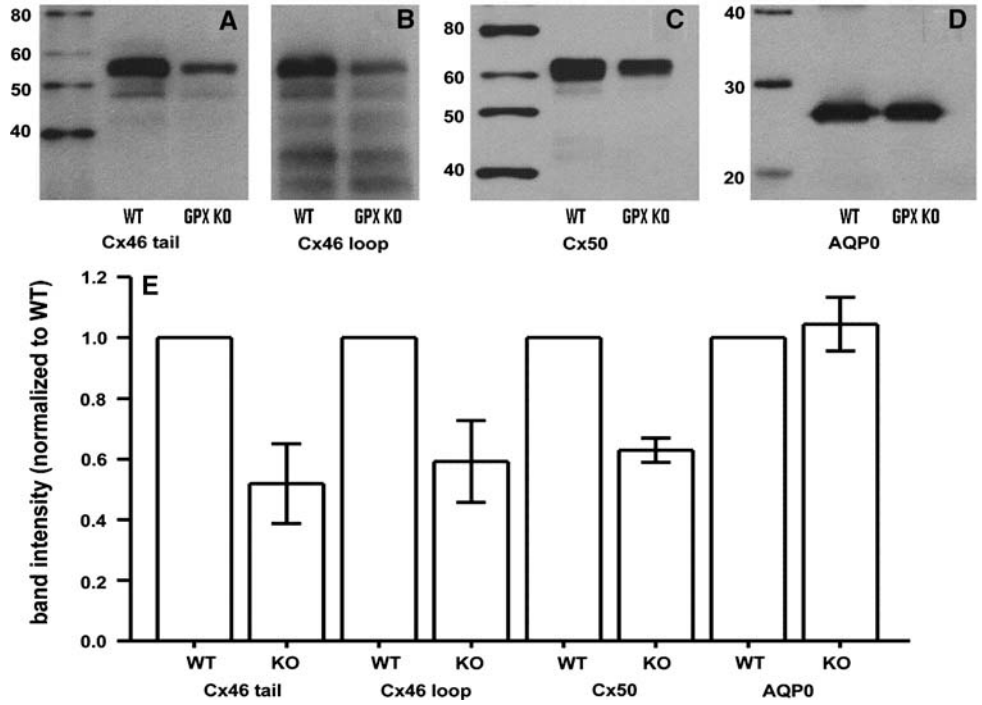

Fig. 5 Western blots of Cx46, Cx50 and AQP0 in WT and GPX-1 KO lenses. Membrane proteins were isolated from the lenses of WT and GPX-1 KO mice as described in "Materials and Methods." **a** Western blot of Cx46 using an antibody to the C terminus, which is cleaved at the DF-MF transition; hence, these data represent DF only. **b** Western blot of Cx46 using an antibody to the inner loop, which is not cleaved; hence, these data represent Cx46 in the DF and MF. The MF contains a number of cleavage products of Cx46, and these products are present in either WT or KO lenses; thus, they represent normal cleavage that appears to be independent of the oxidative damage. **c** Western blot of Cx50 using an antibody to its C terminus, which is cleaved at the DF-MF transition; hence, these data represent DF only. **d** Western blot of AQP0 using an antibody to its C terminus. Though there is some cleavage of AQP0's C terminus with age and internalization within the lens, it is not as abrupt as for the connexins; hence, these data represent uncleaved AQP0 in both DF and MF. **e** Quantitative comparison of the antibody staining in GPX-1 KO relative to WT lenses. Both Cx46 and Cx50 were significantly reduced ($P < 0.05$) in KO lenses, while there was no significant difference in detectable AQP0 ($P = 0.36$). Data are the mean ± SD of three or four blots for each antibody tested

is cleaved at the DF-MF transition, the "Cx46 tail" blot represents just DF protein, whereas the "Cx46 loop" blot represents protein from both DF and MF. In both cases, the amount of immunodetectable protein was reduced in the GPX-1 KO samples. Similar data were obtained using an antibody recognizing Cx50 (Fig. 5c). In contrast, when blots were probed with an antibody recognizing the fiber cell membrane water channel AQP0 (Fig. 5d), there was no decrease in the level of immunodetectable protein.

The bar graph in Fig. 5e compares the intensities of the major bands from WT and GPX-1 KO lenses. The intensity of staining by antibodies to either connexin protein from the KO lenses drops to levels equivalent to 50–60% of WT, consistent with the average drop in coupling conductance seen in Table 1. These data do not show whether the protein has been degraded through some regulatory pathway (Lin and Takemoto 2005) or whether epitopes in the cytoplasmic domains have been directly damaged, causing the antibodies to no longer recognize them. However the data are consistent with the transport data suggesting GPX-1 KO causes loss of coupling conductance due to loss of functional Cx46 and Cx50 gap junction channels. Levels of AQP0 were unchanged between WT and GPX-1 KO lenses, consistent with the water permeability results described in Fig. 4. These results suggest the effects of GPX-1 KO are not general but specific to lens gap junction channels.

Intracellular Ca^{2+} Measurements

Work described by Gao et al. (2004) as well as model calculations suggest reductions in gap junction coupling conductance will cause an increase in the center-to-surface $[Ca^{2+}]_i$ gradient that is present due to electrodiffusion of Ca^{2+}. Figure 6 shows the distribution of intracellular Ca^{2+} in 2-month-old GPX-1 KO and WT lenses. In a single lens, we typically made three to five injections of Fura2 at increasing depths into the lens. Circles are measurements from WT lenses and triangles represent measurements from GPX-1 KO lenses. The smooth curves are fits of Eq. 11 to the data. The curve fits projected the values of calcium concentration at the lens surface—$[Ca^{2+}]_i(a)$—to be

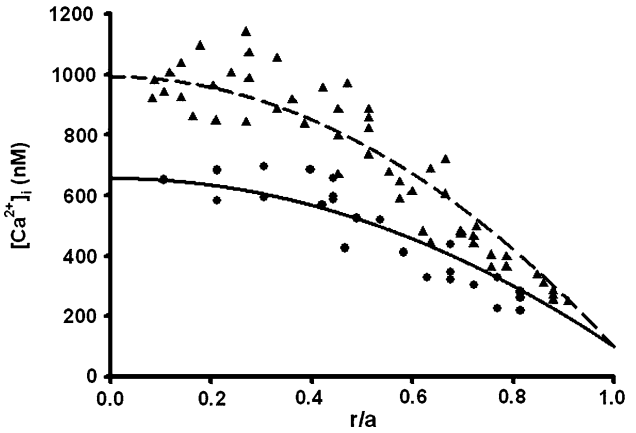

Fig. 6 Comparison of the distribution of $[Ca^{2+}]_i$ in 2-month-old WT and GPX-1 KO lenses. *Black circles* represent $[Ca^{2+}]_i$ data, which were pooled from 12 different 2-month-old WT lenses, each contributing two to five locations. The data follow the *black smooth curve*, which was generated from the electrodiffusion model given in Eq. 11. The radial gradient suggests a flux of calcium flowing from the lens center to surface. *Triangles* are data from 16 different 2-month-old GPX-1 KO lenses. Overall, the MF $[Ca^{2+}]_i$ in 2-month-old GPX-1 KO lenses is higher than that in 2-month-old WT lenses at all depths into the lens but particularly in central fiber cells. However, the KO data were well fit by the electrodiffusion model (*dashed line*), indicating a functional circulation

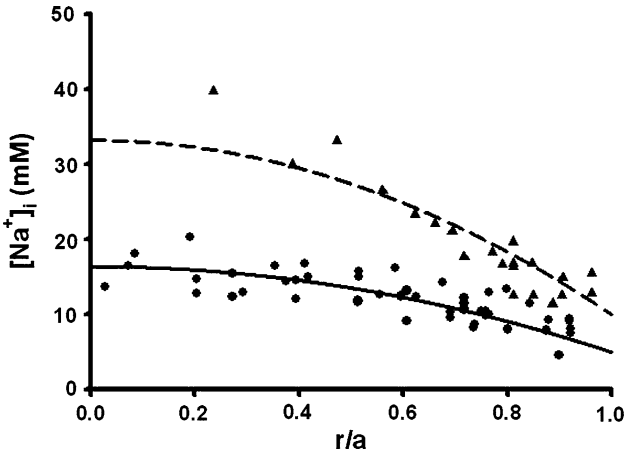

Fig. 7 Comparison of the distribution $[Na^+]_i$ in 2-month-old WT and GPX-1 KO lenses. *Black circles* represent $[Na^+]_i$ data from 12 different 2-month-old WT lenses. The data follow the *black smooth curve* generated from the electrodiffusion model given by Eq. 11. The data suggest a flux of Na^+ from the center to the surface. *Triangles* are data from nine different 2-month-old GPX-1 KO lenses. Overall, the $[Na^+]_i$ in 2-month-old GPX-1 KO lenses is higher than that in 2-month-old WT lenses at all depths into the lens, but the data still follow a smooth diffusion curve (*dashed line*), suggesting the circulation is still functional

100 nM in both WT and GPX-1 KO lenses, suggesting that neither the epithelial Ca-transport systems (Ca ATPase and Na/Ca exchange) nor the Ca^{2+} current into fiber cells were altered by KO of GPX-1 (see "Theory"). The Ca diffusion gradient between the lens surface and center—$\Delta[Ca^{2+}]_i$—was about 556 nM in the control group and 892 nM in the GPX-1 KO group. Thus, halving the coupling conductance almost doubled the diffusion gradient, suggesting the lens circulation is still functional, though at the expense of Ca^{2+} accumulation in central fibers.

Intracellular Na^+ Measurements

If decreases in coupling conductance have caused accumulation of intracellular calcium, they should have a similar effect on intracellular sodium. Figure 7 shows the distribution of intracellular Na^+ as a function of distance from the lens center. Circles represent WT lenses and triangles are data from GPX-1 KO lenses. Overall, the Na^+ concentration in GPX-1 KO lenses is higher than that in WT lenses at all depths into the lens. The values of sodium concentration at the lens surface—$[Na^+]_i(a)$—were 5 mM WT and 10 mM GPX-1 KO, suggesting some reduction in the number of active epithelial Na/K pumps. This is consistent with reports from Spector's lab of H_2O_2-induced damage to lens epithelial Na/K pumps (Garner et al. 1983). The Na gradient between the lens center and surface ($\Delta[Na^+]_i$) was 11 mM in WT and 23 mM in GPX-1 KO mice. Thus, the gradient approximately doubled when coupling was reduced by half, suggesting no significant change in Na^+ influx across fiber cell membranes (see "Theory"). Moreover, the concentration still forms a smooth diffusion gradient, consistent with an active circulation that has nearly normal Na^+ fluxes but that an increase in $\Delta[Na^+]_i$ is required to drive the fluxes.

We assume the cells of these lenses are nearly isosmotic and that macroscopic electroneutrality must hold (Mathias 1985; Mathias et al. 1997, 2007), implying the total concentration of $[Na^+]_i + [K^+]_i$ was essentially spatially uniform. The increase in the core $[Na^+]_i$ must therefore be accompanied by a decrease in $[K^+]_i$. The values of $[K^+]_i$ were not measured, but since the value is typically around 145 mM, a 10-mM decrease would have little effect, particularly since the K^+ conductance is predominantly in the epithelium (Webb and Donaldson 2008), where the GPX-1 KO and WT lenses had the same values of $[Na^+]_i$ and $[K^+]_i$. This assumption is supported by the resting voltage data, which show no significant difference between WT and GPX-1 KO lenses.

Discussion

The earliest detectable effect of GPX-1 KO on lens transport appears to be a reduction in gap junction coupling conductance due to loss of functional Cx46 and Cx50 proteins. The loss of coupling does not appear to reduce the normal lens circulation of ions, at least in these young

lenses; however, the electrochemical gradients driving those fluxes increase, implying that intracellular homeostasis is compromised. As reported by Reddy et al. (2001), lenses from KO mice will eventually develop cataracts. Could this compromise in intracellular homeostasis in young lenses lead to the formation of cataracts in older lenses?

Effects of Ca^{2+} Accumulation

In lenses from young Cx46 KO mice, a cataract forms in central fiber cells, where intracellular Ca^{2+} exceeds 1 μM (Gao et al. 2004), and its formation is dependent on activation of the lens-specific calpain Lp82 (Tang et al. 2007; Baruch et al. 1992). Lenses from young GPX-1 KO mice are transparent, but intracellular Ca^{2+} has accumulated to very near 1 μM in their central fiber cells. This level of Ca^{2+} has most likely caused calpain activity to increase over that in WT lenses. Lenses, however, have protective mechanisms, such as α-crystallin-mediated chaperone activity (Horwitz et al. 1999), which can prevent aggregation of cleaved proteins as long as the damage is not too extensive. Possibly, this is what is happening in the GPX-1 KO lenses. When the KO lenses get older, the accumulation of cleaved proteins could eventually overwhelm the ability of chaperones; hence, cataracts form. Thus, accumulation of Ca^{2+} alone could be sufficient cause for the eventual cataract; however, there are probably other factors that contribute.

Effects of Na^+ Accumulation

Na^+ is thought to be the major ion driving the lens circulation (Mathias et al. 2007). Reductions in gap junction coupling in GPX-1 KO lenses were therefore expected to cause accumulation of Na^+ in central fiber cells, as was observed. The increase in the center-to-surface Na^+ gradient, $\Delta[Na^+]_i$, was approximately proportional to the decrease in coupling conductance, suggesting no significant change in Na^+ flux; hence, there should have been no significant change in fluid transport or the delivery of essential nutrients, amino acids and antioxidants to central fiber cells. However, the membrane transporters for these molecules are often cotransporters, which rely on the transmembrane electrochemical gradient for Na^+ to drive uptake of the molecule (reviewed in Mathias et al. 2007). Thus, even though the circulation still appears functional in the young GPX-1 KO lenses, there will be reductions in the capacity to transport important molecules into central fiber cells.

For example, sodium-dependent glucose uptake by SGLT2 was observed in fiber cells (Merriman-Smith et al. 1999, 2003; Donaldson et al. 2001). Sodium-dependent amino acid transporters in lens fiber cells include the excitatory amino acid transporters (EAAT4/5), the alanine serine cysteine transporter (ASCT2) and the glycine transporter (GLYT1) (Lim et al. 2005, 2006), all of which help to accumulate amino acids in the lens core. Glutathione (GSH) is synthesized from the amino acids cysteine, glutamate and glycine (Beutler, 1989; Deneke and Fanburg 1989). In the MF, where little GSH is synthesized, cysteine may function as an antioxidant by maintaining proteins in their reduced state (Lou 2003). Accumulation of Na^+ in fiber cells will diminish the capacity of all of these transporters, thus contributing to eventual loss of homeostasis and a cataract.

Oxidative Damage, Calcium and Cataracts

Elevated Ca^{2+} and extensive oxidative damage have often been associated with lenses from patients with cataracts (Spector 1995; Duncan and van Heyningen 1977; Jacob 1983; Stark 2005; Truscott 2005). However, cataractous lenses have already lost homeostasis, so it has not been clear whether these factors were a cause or a consequence of loss of homeostasis.

Duncan and Bushell (1975) reported that cortical cataracts had grossly increased total calcium concentrations, while nuclear cataracts had a near normal range of total calcium concentrations. However, many other investigators have reported a wide range of total lens calcium content in different types of cataracts (Tang et al. 2003). These studies measured total-lens Ca^{2+}, which includes both intracellular and extracellular Ca^{2+}. The volume fraction of a healthy lens that is extracellular is only about 1/100, but the concentration of extracellular Ca^{2+} is at least 1,000 times greater than that of intracellular Ca^{2+}; thus, large increases in total Ca^{2+} are likely to be associated with cellular damage and expansion of the extracellular volume within the lens. A large elevation in total-lens Ca^{2+} is therefore likely to be a consequence of loss of homeostasis. In the studies reported here, we measured the spatial distribution of free intracellular Ca^{2+}, which is a small fraction of total-lens Ca^{2+}. The increase in intracellular Ca^{2+} that we found may indeed be a causal factor in the cataract that would eventually form in all of the GPX-1 KO lenses (Reddy et al. 2001).

Previous work suggested that oxidative damage to lens proteins is involved in the development of cataracts (Spector 1984). Oxidative agents include UV radiation, O_2 and H_2O_2. H_2O_2 is probably a major oxidant that leads to protein damage in lenses since it has a relatively high concentration in the aqueous and vitreous humors. GPX-1 KO mice lack an important protective enzyme against H_2O_2-mediated oxidative damage, so one assumes these lenses are subjected to higher levels of damage than WT lenses, though other indirect effects could also affect these

lenses. Nevertheless, GPX-1 KO lenses support the hypothesis that oxidative damage is a cause of central cataracts as they develop age-dependent central cataracts (Reddy et al. 2001). Thus, oxidative damage appears to be a likely cause of cataract rather than a consequence of loss of homeostasis, though the extensive oxidative damage seen in cataractous lenses may be due to both.

Summary

Cataract is a loss of intracellular homeostasis. Although there can be numerous causes for such a loss, accumulation of oxidative damage is most likely the cause of the eventual cataracts in GPX-1 KO lenses. Intracellular homeostasis depends on membrane transport, so it is not surprising that damage to membrane transport precedes cataract formation in these lenses. Homeostasis in the MF depends on the lens circulation and, hence, on gap junction coupling, which appears to be particularly susceptible to damage in the GPX-1 KO lenses. While we have studied just GPX-1 KO lenses, damage to membrane transport, particularly to lens connexins, might be a general theme in the formation of age-dependent central cataracts.

Acknowledgements This work was supported by NIH grants EY06391 and EY13163.

References

Baldo GJ, Gong X, Martinez-Wittinghan FJ, Kumar NM, Gilula NB, Mathias RT (2001) Gap junctional coupling in lenses from alpha(8) connexin knockout mice. J Gen Physiol 118(5):447–456

Baldo GJ, Mathias RT (1992) Spatial variations in membrane properties in the intact rat lens. Biophys J 63(2):518–529

Baruch A, Greenbaum D, Levy ET, Nielsen PA, Gilula NB, Kumar NM, Bogyo M (2001) Defining a link between gap junction communication, proteolysis, and cataract formation. J Biol Chem 276(31):28999–29006

Bassnett S, Beebe DC (1992) Coincident loss of mitochondria and nuclei during lens fiber cell differentiation. Dev Dyn 194(2):85–93

Beutler E (1989) Nutritional and metabolic aspects of glutathione. Annu Rev Nutr 9:287–302

Candia OA, Alverez JL (2006) Water and ion transport in ocular tissues. Physiol Mini-Rev 1:48–57

Candia OA, Zamudio AC (2002) Regional distribution of the Na^+ and K^+ currents around the crystalline lens of rabbit. Am J Physiol 282(2):C252–C262

Delamere NA, Tamiya S (2004) Expression, regulation and function of Na, K-ATPase in the lens. Prog Retin Eye Res 23(6):593–615

Deneke SM, Fanburg BL (1989) Regulation of cellular glutathione. Am J Physiol 257(4 Pt 1):L163–L173

DeRosa AM, Mui R, Srinivas M, White TW (2006) Functional characterization of a naturally occurring Cx50 truncation. Invest Ophthalmol Vis Sci 47(10):4474–4481

Donaldson P, Kistler J, Mathias RT (2001) Molecular solutions to mammalian lens transparency. News Physiol Sci 16:118–123

Duncan G, Bushell AR (1975) Ion analyses of human cataractous lenses. Exp Eye Res 20(3):223–230

Duncan G, van Heyningen R (1977) Distribution of non-diffusible calcium and sodium in normal and cataractous human lenses. Exp Eye Res 25(2):183–193

Eisenberg RS, Barcilon V, Mathias RT (1979) Electrical properties of spherical syncytia. Biophys J 25(1):151–180

Gao J, Sun X, Yatsula V, Wymore RS, Mathias RT (2000) Isoform-specific function and distribution of Na/K pumps in the frog lens epithelium. J Membr Biol 178(2):89–101

Gao J, Sun X, Martinez-Wittinghan FJ, Gong X, White TW, Mathias RT (2004) Connections between connexins, calcium, and cataracts in the lens. J Gen Physiol 124(4):289–300

Garner WH, Garner MH, Spector A (1983) H2O2-induced uncoupling of bovine lens Na^+, K^+-ATPase. Proc Natl Acad Sci USA 80(7):2044–2048

Gonen T, Sliz P, Kistler J, Cheng Y, Walz T (2004) Aquaporin–0 membrane junctions reveal the structure of a closed water pore. Nature 429(6988):193–197

Gong X, Li E, Klier G, Huang Q, Wu Y, Lei H, Kumar NM, Horwitz J, Gilula NB (1997) Disruption of alpha3 connexin gene leads to proteolysis and cataractogenesis in mice. Cell 91(6):833–843

Gong X, Baldo GJ, Kumar NM, Gilula NB, Mathias RT (1998) Gap junctional coupling in lenses lacking alpha3 connexin. Proc Natl Acad Sci USA 95(26):15303–15308

Goodenough DA, Goliger JA, Paul DL (1996) Connexins, connexons, and intercellular communication. Annu Rev Biochem 65: 475–502

Horwitz J, Bova MP, Ding LL, Haley DA, Stewart PL (1999) Lens alpha-crystallin: function and structure. Eye 13(Pt 3b):403–408

Jacob TJ (1983) Raised intracellular free calcium within the lens causes opacification and cellular uncoupling in the frog. J Physiol 341:595–601

Kumar NM, Gilula NB (1996) The gap junction communication channel. Cell 84(3):381–388

Kuszak JR, Rae JL (1982) Scanning electron microscopy of the frog lens. Exp Eye Res 35(5):499–519

Lim J, Lam YC, Kistler J, Donaldson PJ (2005) Molecular characterization of the cystine/glutamate exchanger and the excitatory amino acid transporters in the rat lens. Invest Ophthalmol Vis Sci 46(8):2869–2877

Lim J, Lorentzen KA, Kistler J, Donaldson PJ (2006) Molecular identification and characterisation of the glycine transporter (GLYT1) and the glutamine/glutamate transporter (ASCT2) in the rat lens. Exp Eye Res 83(2):447–455

Lin D, Takemoto DJ (2005) Oxidative activation of protein kinase Cgamma through the C1 domain. Effects on gap junctions. J Biol Chem 280(14):13682–13693

Lou MF (2003) Redox regulation in the lens. Prog Retin Eye Res 22(5):657–682

Martinez-Wittinghan FJ, Sellitto C, White TW, Mathias RT, Paul D, Goodenough DA (2004) Lens gap junctional coupling is modulated by connexin identity and the locus of gene expression. Invest Ophthalmol Vis Sci 45(10):3629–3637

Martinez-Wittinghan FJ, Srinivas M, Sellitto C, White TW, Mathias RT (2006) Mefloquine effects on the lens suggest cooperative gating of gap junction channels. J Membr Biol 211(3):163–171

Mathias RT (1985) Steady-state voltages, ion fluxes, and volume regulation in syncytial tissues. Biophys J 48(3):435–448

Mathias RT, Rae JL (1985) Transport properties of the lens. Am J Physiol 249(3 Pt 1):C181–C190

Mathias RT, Riquelme G, Rae JL (1991) Cell to cell communication and pH in the frog lens. J Gen Physiol 98(6):1085–1103

Mathias RT, Rae JL, Baldo GJ (1997) Physiological properties of the normal lens. Physiol Rev 77(1):21–50

Mathias RT, Kistler J, Donaldson P (2007) The lens circulation. J Membr Biol 216(1):1–16

Merriman-Smith R, Donaldson P, Kistler J (1999) Differential expression of facilitative glucose transporters GLUT1 and GLUT3 in the lens. Invest Ophthalmol Vis Sci 40(13):3224–3230

Merriman-Smith BR, Krushinsky A, Kistler J, Donaldson PJ (2003) Expression patterns for glucose transporters GLUT1 and GLUT3 in the normal rat lens and in models of diabetic cataract. Invest Ophthalmol Vis Sci 44(8):3458–3466

Parmelee JT (1986) Measurement of steady currents around the frog lens. Exp Eye Res 42(5):433–441

Paul DL, Ebihara L, Takemoto LJ, Swenson KI, Goodenough DA (1991) Connexin46, a novel lens gap junction protein, induces voltage-gated currents in nonjunctional plasma membrane of *Xenopus* oocytes. J Cell Biol 115(4):1077–1089

Reddy VN (1990) Glutathione and its function in the lens-an overview. Exp Eye Res 50(6):771–778

Reddy VN, Giblin FJ, Lin LR, Dang L, Unakar NJ, Musch DC, Boyle DL, Takemoto LJ, Ho YS, Knoernschild T, Juenemann A, Lutjen-Drecoll E (2001) Glutathione peroxidase-1 deficiency leads to increased nuclear light scattering, membrane damage, and cataract formation in gene-knockout mice. Invest Ophthalmol Vis Sci 42(13):3247–3255

Robinson KR, Patterson JW (1982–1983) Localization of steady currents in the lens. Curr Eye Res 2(12):843–847

Shiels A, Bassnett S, Varadaraj K, Mathias R, Al-Ghoul K, Kuszak J, Donoviel D, Lilleberg S, Friedrich G, Zambrowicz B (2001) Optical dysfunction of the crystalline lens in aquaporin-0-deficient mice. Physiol Genomics 7(2):179–186

Spector A (1984) Oxidation and cataract. Ciba Found Symp 106: 48–64

Spector A (1995) Oxidative stress-induced cataract: mechanism of action. FASEB J 9(12):1173–1182

Spray DC, Harris AL, Bennett MV (1981) Gap junctional conductance is a simple and sensitive function of intracellular pH. Science 211(4483):712–715

Stark G (2005) Functional consequences of oxidative membrane damage. J Membr Biol 205(1):1–16

Tang D, Borchman D, Yappert MC, Vrensen GF, Rasi V (2003) Influence of age, diabetes, and cataract on calcium, lipid–calcium, and protein–calcium relationships in human lenses. Invest Ophthalmol Vis Sci 44(5):2059–2066

Tang D, Liu X, Soltoski RK, Novak LA, Herrera RA, Richard I, Kuszak JR, Kumar NM (2007) Age-related cataracts in alpha 3 Cx46-knockout mice are dependent on a calpain 3 isoform. Invest Ophthalmol Vis Sci 48(6):2685–2694

Truscott RJ (2005) Age-related nuclear cataract-oxidation is the key. Exp Eye Res 80(5):709–725

Varadaraj K, Kushmerick C, Baldo GJ, Bassnett S, Shiels A, Mathias RT (1999) The role of MIP in lens fiber cell membrane transport. J Membr Biol 170(3):191–203

Webb KF, Donaldson PJ (2008) Differentiation-dependent changes in the membrane properties of fiber cells isolated from the rat lens. Am J Physiol 294(5):C1133–C1145